法政大学学術機関リポジトリ

HOSEI UNIVERSITY REPOSITORY

Spin-dependent three-nucleon force effects on nucleon-deuteron scattering

	Ishikawa Souichi
	The American Physical Society
journal or publication title	Physical Review C
page range	061002-1-061002-5
year	2007-06-21
URL	http://hdl.handle.net/10114/1247

Spin-dependent three-nucleon force effects on nucleon-deuteron scattering

S. Ishikawa[*]

Department of Physics, Science Research Center, Hosei University, 2-17-1 Fujimi, Chiyoda, Tokyo 102-8160, Japan and
Triangle Universities Nuclear Laboratory, Durham, North Carolina 27708-0308, USA
(Received 14 March 2007; published 21 June 2007)

We construct a phenomenological three-nucleon force (3NF) model that gives a good description of polarization observables in elastic nucleon-deuteron (N-d) scattering at a low energy together with a realistic nucleon-nucleon force and a 3NF arising from the exchange of two pions. Parameters of the model, which consists of spin-independent, spin-orbit, and tensor components, are determined to reproduce the three-nucleon binding energy and polarization observables in N-d scattering at 3 MeV. Predictions of the 3NF model on N-d polarization observables at higher energies are examined, and the effects of each component on the observables are investigated.

As is well known, modern two-nucleon force (2NF) models have a deficiency in explaining the binding energies of three-nucleon (3N) systems, and this problem is successfully solved by introducing a 3NF arising from the exchange process of two pions among three nucleons, which is called the two-pion-exchange (2πE) 3NF [1,2]. However, such combinations of the 2NFs and the 2πE-3NF that reproduce the 3N binding energy do not necessarily explain polarization observables in 3N scattering systems such as vector or tensor analyzing powers in elastic N-d scattering. See, e.g., Table III of Ref. [3], where calculations of observables with and without a 2πE-3NF are compared in terms of χ^2 with experimental data below 30 MeV of incident nucleon energy in the laboratory system. In spite of recent progress in constructing realistic 3NFs from chiral effective field theory or from heavier-boson-exchange mechanisms, no consensus has been obtained for possible mechanisms of 3NFs consistent with all of the experimental data. On the other hand, model 3NFs with artificial functional forms have been proposed to explain the polarization observables quite well [4–6]. These 3NFs have a form that typical components in 2NFs, e.g., central spin-independent, tensor, or spin-orbit components, are modified in the presence of third nucleon. [See Eq. (1) below.]

In this paper, we introduce such a phenomenological 3NF to resolve the discrepancies of a 2NF and the 2πE-3NF at a low energy, and we examine whether it is still valid for N-d observables at higher energies up to 30 MeV. Since it may not be so difficult to understand what physical process is simulated by the spin dependence of each component, we expect that the present study will provide some hint of which characteristics of more realistic 3NFs should be studied.

Our 3N calculations are based on a formalism to solve the Faddeev equations in coordinate space as integral equations [7,8]. For scattering states below the 3N breakup threshold energy, effects of the long-range Coulomb force between two

protons are exactly treated [9]. Calculations for energies above the 3N breakup threshold are formulated in Ref. [10]. 3N partial wave states for which 2NFs and 3NFs act, are restricted to those with total two-nucleon angular momenta $j \leqslant 6$ for bound state calculations, and $j \leqslant 3$ for scattering state calculations. The total 3N angular momentum is truncated at $J = 19/2$, while 3NFs are switched off for 3N states with $J > 9/2$. These truncating procedures are confirmed to give converged results for the purposes of the present work.

We use the Argonne V_{18} model (AV18) [11] for the realistic 2NF and the Brazil model (BR) [2] for the 2πE-3NF. Calculated triton binding energies with models used in this work are tabulated in Table I. The AV18 calculation underbinds the triton by about 0.9 MeV. The introduction of the 2πE-3NF produces enough attraction to remedy the defect, but it strongly depends on the choice of cutoff parameter in the πNN form factor. We choose a dipole form factor, $(\frac{\Lambda^2 - m_\pi^2}{q^2 + \Lambda^2})^2$, where $\boldsymbol{q}$ is the momentum of the exchanged pion, m_π the pion mass, and Λ the cutoff mass. The choice of $\Lambda = 800$ MeV $\approx 5.8 m_\pi$ (BR$_{800}$), which is close to a value cited in Refs. [2,12,13] to explain the Goldberger-Treiman discrepancy, overshoots the triton binding energy by about 0.9 MeV. It turns out that the binding energy is reproduced when we take $\Lambda = 680$ MeV $\approx 4.9 m_\pi$ (BR$_{680}$). This rather small value of Λ may be considered as the result of incorporating unknown 3NF effects.

As examples to demonstrate the effects of 3NFs at low energy, we show our calculations for the proton vector analyzing power $A_y(\theta)$ and the deuteron tensor analyzing power $T_{21}(\theta)$ in elastic proton-deuteron (p-d) scattering at $E_p = 3.0$ MeV (or $E_d = 6.0$ MeV) in Fig. 1, comparing them with experimental data [14,15]. Deficiencies of the AV18 calculations in reproducing the data prominently appear as a smallness for the maximum of $A_y(\theta)$ at $\theta \approx 100°$ and as an excess for the local minimum of $T_{21}(\theta)$ at $\theta \approx 80°$. The AV18+BR$_{800}$ and the AV18+BR$_{680}$ calculations, which almost agree, demonstrate that the 2πE-3NF partially remedies the deficiency of the A_y maximum but worsens that of the T_{21} minimum. In Ref. [5], the latter effect was shown to arise from a tensor component in the 2πE-3NF.

---

*ishikawa@hosei.ac.jp

TABLE I. Empirical value and calculated values of the triton binding energy (B_3). See the text for the description of the models.

Model	B_3 (MeV)
Empirical	8.482
AV18	7.626
AV18+BR$_{800}$	9.380
AV18+BR$_{680}$	8.493
AV18+BR$_{800}$+C+T+SO	8.478
AV18+BR$_{680}$+SO	8.444

Now we consider a phenomenological 3NF to improve the results of AV18+BR$_{800}$ in Fig. 1 in the following form [4–6],

$$V = \sum_{i<j} e^{-(\frac{r_{ik}}{r_G})^2 - (\frac{r_{jk}}{r_G})^2} \{V_0 + V_T S_T(ij)\hat{P}_{11}(ij)\}$$
$$+ V_{ls} e^{-\alpha\rho} \sum_{i<j} [l_{ij} \cdot (S_i + S_j)]\hat{P}_{11}(ij), \tag{1}$$

where $S_T(ij)$ is the tensor operator acting between nucleon pair (i, j), $\hat{P}_{11}(ij)$ the projection operator to the spin and isospin triplet state of the (i, j) pair, and $\rho^2 = \frac{2}{3}(r_{12}^2 + r_{23}^2 + r_{31}^2)$. In the present work, the range parameter r_G is taken to be 1.0 fm as in Refs. [5,6], and α to be 1.5 fm^{-1}, which is the shortest one in Ref. [4]. The parameters for the strength of the central spin-independent component (C) V_0, the tensor component (T) V_T, and the spin-orbit component (SO) V_{ls} are determined to reproduce the triton binding energy and the observables in Fig. 1 as follows: In Ref. [6], it is reported that one can simulate the 2πE-3NF by Eq. (1) with a choice of $(V_0, V_T) = (-38$ MeV, $+20$ MeV$)$, and then get a remarkable improvement in $T_{21}(\theta)$ by changing the sign of V_T and readjusting V_0 to fit the triton binding energy. Thus, in the present case, we choose the variation $-20 - (+20) =$

-40 MeV for the value of V_T to improve $T_{21}(\theta)$ in addition to AV18+BR$_{800}$. Hereafter, we call this procedure *tensor inversion*. The strength of the spin-orbit component V_{ls} is determined to be -16 MeV to reproduce $A_y(\theta)$ at 3.0 MeV. Finally, the strength of the spin-independent component V_0 is determined to reproduce the triton binding energy. The values obtained are $(V_0, V_T, V_{ls}) = (+25, -40, -16$ MeV$)$. The results of this 3NF (AV18+BR$_{800}$+C+T+SO) are displayed as the solid curves in Fig. 1.

We note here that the C-3NF plays an essential role in reproducing the binding energy to get the repulsive effect against the large attraction from the BR$_{800}$-3NF. To the total repulsion of about 0.90 MeV by the C+T+SO-3NF (see Table I), the C-3NF contributes about 0.62 MeV, the T-3NF about 0.24 MeV, and the SO-3NF 0.05 MeV.

To understand the role of the tensor inversion, we make another model 3NF so that $A_y(\theta)$ at 3.0 MeV is reproduced with AV18+BR$_{680}$ plus Eq. (1) with $V_0 = V_T = 0$, which will be denoted as AV18+BR$_{680}$+SO. In this case, the strength of the SO term becomes $V_{ls} = -21$ MeV. Since the effect of the SO-3NF on the triton binding energy is rather small, about 0.05 MeV of repulsive contribution, AV18+BR$_{680}$+SO reproduces the binding energy as well. In Fig. 1, the results of AV18+BR$_{680}$+SO are not plotted because they coincide with the AV18+BR$_{800}$+C+T+SO calculation for $A_y(\theta)$ and with AV18+BR$_{680}$ for $T_{21}(\theta)$. Note that the latter demonstrates that the SO-3NF has only a minor effect on $T_{21}(\theta)$.

In Fig. 2, we show the results of calculations of the tensor analyzing power $T_{21}(\theta)$ in elastic neutron-deuteron (n-d) scattering at $E_n = 28.0$ MeV (or $E_d = 56.0$ MeV) compared with p-d data at the corresponding energy [16], for which the effect of the Coulomb force may be small as shown in Ref. [3]. In this energy, the AV18 calculation looks to be almost in agreement with the data. However, the
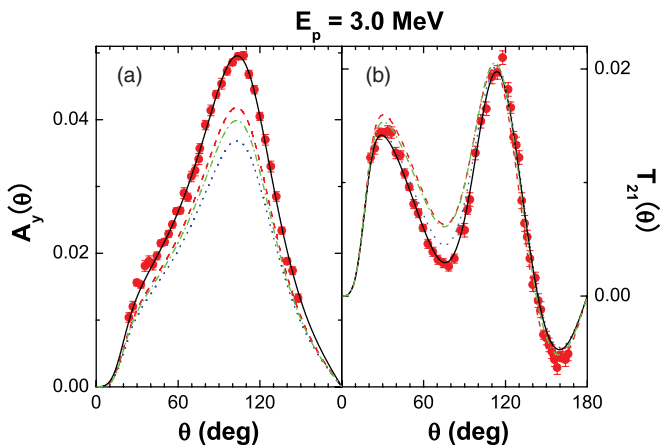

FIG. 1. (Color online) (a) Proton vector analyzing power $A_y(\theta)$ and (b) deuteron tensor analyzing power $T_{21}(\theta)$ in p-d scattering at $E_p = 3.0$ MeV ($E_d = 6.0$ MeV). Dotted (blue) curves denote the AV18 calculations; dashed (red) curves, AV18+BR$_{800}$; dotted-dashed (green) curves, AV18+BR$_{680}$; solid (black) curves, AV18+BR$_{800}$+C+T+SO. Solid circles are experimental data from Refs. [14,15].
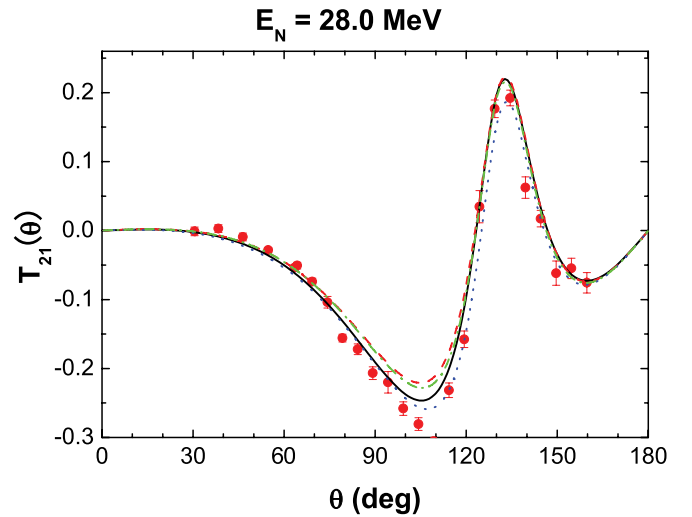

FIG. 2. (Color online) Deuteron tensor analyzing power $T_{21}(\theta)$ in N-d scattering at $E_N = 28.0$ MeV (or $E_d = 56.0$ MeV). Calculations are for n-d: dotted (blue) curve denotes the AV18 calculation; dashed (red) curve AV18+BR$_{680}$+SO; dotted-dashed (green) curve AV18+BR$_{680}$; solid (black) curve AV18+BR$_{800}$+C+T+SO. Solid circles are experimental data for p-d scattering from Ref. [16].
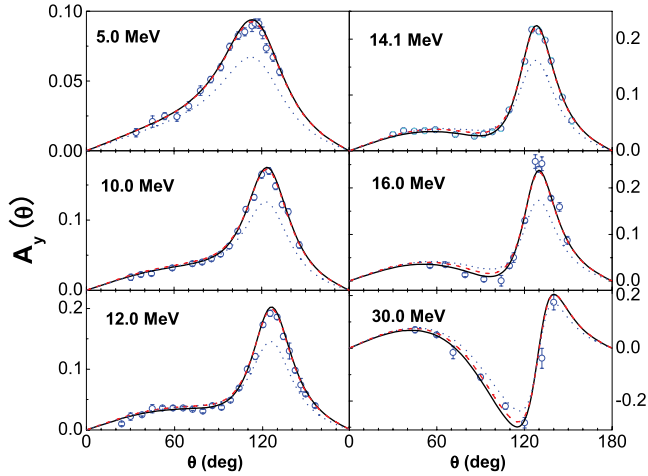
FIG. 3. (Color online) Neutron vector analyzing power $A_y(\theta)$ in n-d scattering. Dotted (blue) curves denote the AV18 calculations; dashed (red) curves, AV18+BR$_{680}$+SO; solid (black) curves, AV18+BR$_{800}$+C+T+SO. Experimental data are from Ref. [17] for 5.0 MeV; Ref. [18] for 10.0; Ref. [19] for 14.1; Ref. [20] for 16.0; and Ref. [21] for 30.0.

introduction of the 2πE-3NF destroys the fit as demonstrated by the dotted-dashed curve. The small difference between AV18+BR$_{680}$ and AV18+BR$_{680}$+SO shows that the SO-3NF plays only a minor role in this observable as well as for 3.0 MeV. On the other hand, the tensor inversion effect almost cancels the unfavorable effect due to the 2πE-3NF. Note that the effect of the tensor inversion in this energy is different from that in 3.0 MeV, which overshoots the effect of 2πE-3NF, although both effects are favorable in explaining the data. This difference may occur because of a partial cancellation between the effect of the C-3NF and that of the T-3NF at higher energies.

In Fig. 3, we plot results of the neutron vector analyzing power $A_y(\theta)$ in n-d scattering compared with available experimental data at several energies up to 30 MeV [17–21]. First, we take an overview of the energy dependence in the $A_y(\theta)$ angular distribution. For lower energies, $A_y(\theta)$ has a single peak at $\theta \approx 100°$. As the energy increases, the angle where $A_y(\theta)$ takes the maximum, θ_{max}, increases gradually up to about $140°$ at $E_n = 30$ MeV, and a plateau region appears at $\theta \approx 90°$ for $E_n \geqslant 10$ MeV developing into a local minimum.

Failures of the AV18 calculations in reproducing the minimum and maximum of the $A_y(\theta)$ data are well recovered by the AV18+BR$_{800}$+C+T+SO and the AV18+BR$_{680}$+SO calculations. This is essentially because of the contribution from the SO-3NF.

A closer look at Fig. 3 shows that the AV18+BR$_{800}$+C+T+SO and the AV18+BR$_{680}$+SO calculations equivalently reproduce the A_y maximum, but they display a difference at higher energies for angles $80° \leqslant \theta \leqslant 120°$, where $A_y(\theta)$ has the local minimum. To emphasize this, we plot in Fig. 4 the values of $A_y(\theta)$ at $\theta = 90°$ and those at θ_{max} as a function of the incident neutron energy E_n, comparing them with values extracted from the experimental data [17–21]. This figure clearly shows that the effect of the SO-3NF, which is displayed by the difference between the AV18+BR$_{680}$ and the AV18+BR$_{680}$+SO calculations, tends
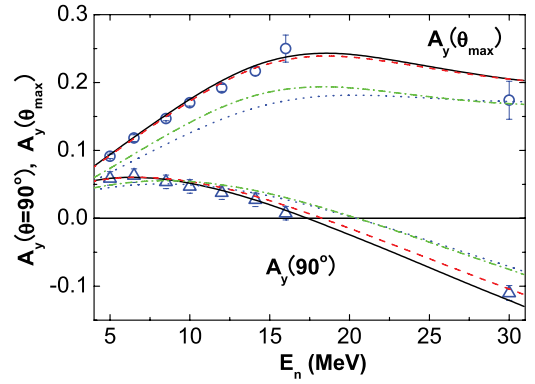

FIG. 4. (Color online) Neutron vector analyzing power $A_y(\theta)$ at $\theta = 90°$ and $\theta = \theta_{max}$ in n-d scattering. Dotted (blue) curves denote the AV18 calculations; dotted-dashed (green) curves, AV18+BR$_{680}$; dashed (red) curves, AV18+BR$_{680}$+SO; solid (black) curves, AV18+BR$_{800}$+C+T+SO. Points are calculated from experimental data [17–21].

to improve $A_y(\theta)$ dominantly at both angles. On the other hand, the tensor inversion effect, displayed by the difference between AV18+BR$_{680}$+SO and AV18+BR$_{800}$+C+T+SO, is small at θ_{max}, but gives a nonnegligible contribution at $\theta = 90°$ as the energy increases, which works in the same direction as the SO-3NF.

As an another interesting example, we pick up nucleon-to-nucleon polarization transfer coefficients in the $\vec{N} + d \rightarrow \vec{N} + d$ reaction, $K_x^{x'}(\theta)$, $K_y^{y'}(\theta)$, $K_z^{z'}(\theta)$, $K_x^{z'}(\theta)$, and $K_z^{x'}(\theta)$. In Fig. 5, calculations of these observables at $E_n = 19.0$ MeV for $60° \leqslant \theta \leqslant 140°$, where calculations of different models scatter, are displayed and compared with experimental data of
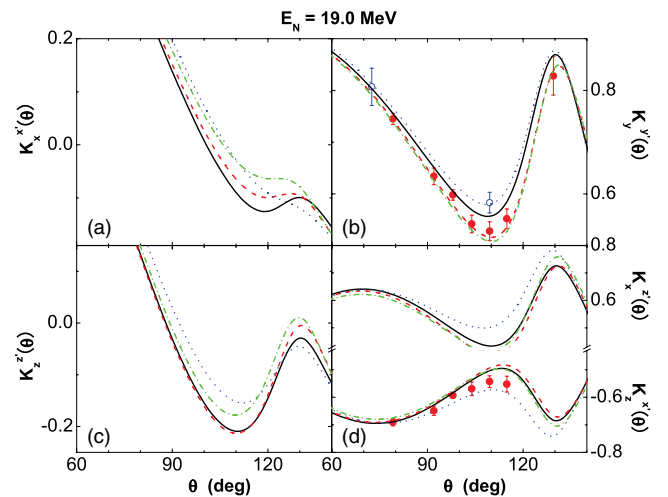

FIG. 5. (Color online) Nucleon-to-nucleon polarization transfer coefficients (a) $K_x^{x'}(\theta)$, (b) $K_y^{y'}(\theta)$, (c) $K_z^{z'}(\theta)$, and (d) $K_x^{z'}(\theta)$ (upper) and $K_z^{x'}(\theta)$ (lower) in N-d scattering at $E_N = 19.0$ MeV. Calculations are for n-d: dotted (blue) curves denote the AV18 calculations; dotted-dashed (green) curves, AV18+BR$_{680}$; dashed (red) curves, AV18+BR$_{680}$+SO; solid (black) curves, AV18+BR$_{800}$+C+T+SO. Open circles in (b) are experimental data for n-d $K_y^{y'}(\theta)$ [22]; solid circles in (b), p-d $K_y^{y'}(\theta)$ [23]; solid circles in (d), p-d $K_z^{x'}(\theta)$ [23].

$K_y^{y'}(\theta)$ for n-d scattering [22] and those of $K_y^{y'}(\theta)$ and $K_z^{x'}(\theta)$ for p-d scattering [23].

For $K_y^{y'}(\theta)$, the calculations and n-d data show tendencies similar to those of $T_{21}(\theta)$ in Fig. 2, namely, the smallness of the SO-3NF effect and the partial cancellation of the 2πE-3NF effect by the tensor inversion. It is likely that the tensor inversion effect works nicely in reproducing the n-d data. However, the position of the n-d data point at $\theta = 110°$ in Fig. 5(b), which is above the p-d data point, is contradictory to the Kohn variational principle calculations with or without including a Coulomb force effect [24]. Therefore, it is not conclusive whether the tensor inverse effect is favorable until more experimental data are accumulated and/or Coulomb effects are fixed.

Figure 5 displays another features of the observables: $K_x^{x'}(\theta)$ and $K_z^{z'}(\theta)$ reveal the dependence on both the tensor inversion and the SO-3NF. On the other hand, $K_x^{z'}(\theta)$ and $K_z^{x'}(\theta)$ do a scaling behavior, i.e., the results with models that equally reproduce the triton binding energy almost agree with each other.

Some of these characteristics may be understood in the following way: In Ref. [25], N-d observables $K_x^x(\theta)$, etc., are analyzed in terms of N-d scattering amplitudes, which are decomposed into scalar, vector, tensor, etc., in spin space. Analyses in Appendix B 8 of Ref. [25] show that $K_x^x(\theta)$ and $K_z^x(\theta)$ are proportional to both vector and tensor components in N-d amplitudes, which are sensitive to spin-orbit and tensor forces, respectively, and that $K_x^x(\theta)$ and $K_z^z(\theta)$ are governed by scalar components leading to the scaling behavior because of their sensitivity to the overall attraction of the nuclear forces. Note that we deal with two different sets of the observables referring to two different coordinate systems: (x, y, z) and (x', y', z'). The former (latter) system is defined so that the z axis (z' axis) is oriented in the direction of the beam (observed) particle. In the N-d elastic scattering, a scattering angle of $\theta = 120°$, around which we are interested in, corresponds to a scattering angle of $90°$ in laboratory system. In this particular angle, it is easily shown that relations: $\hat{x}' = -\hat{z}$, $\hat{y}' = \hat{y}$, and $\hat{z}' = \hat{x}$ hold, and thus we have, $K_x^{x'}(\theta) = -K_x^z(\theta)$, $K_z^{z'}(\theta) = K_x^x(\theta)$, $K_x^{z'}(\theta) = K_z^x(\theta)$, and $K_z^{x'}(\theta) = -K_z^z(\theta)$. This lead to the features of $K_x^{x'}(\theta)$, $K_z^{z'}(\theta)$, $K_x^{z'}(\theta)$, and $K_z^{x'}(\theta)$ around $\theta = 120°$ are originated from as reflections of those of $K_x^z(\theta)$, $K_z^x(\theta)$, $K_x^x(\theta)$, and $K_z^z(\theta)$, respectively.

Final examples of observables that are sensitive to our model 3NFs are spin-dependent total cross section differences in $\vec{n}-\vec{d}$ scattering, $\Delta\sigma_L$ and $\Delta\sigma_T$ [26,27]. These observables are particularly interesting because they are related directly to the imaginary part of n-d scattering amplitudes at forward angle by the optical theorem. In Fig. 6(a), we show calculations of $\Delta\sigma_L$ and $\Delta\sigma_T$ as well as recent measurements of $\Delta\sigma_L$ [26]. In Ref. [27], it is pointed out that the difference $\Delta\sigma_T - \Delta\sigma_L$ is proportional to the imaginary part of a tensor component in the n-d scattering amplitudes at forward angle. As Fig. 6(b) shows, the calculations of the difference for AV18+BR$_{800}$+C+T+SO and AV18+BR$_{680}$+SO are opposite to those of the AV18 calculation, which means the tensor inversion effect is observed clearly. Thus, precise measurements of these observables are of interest in obtaining information about tensor components in 3NFs.
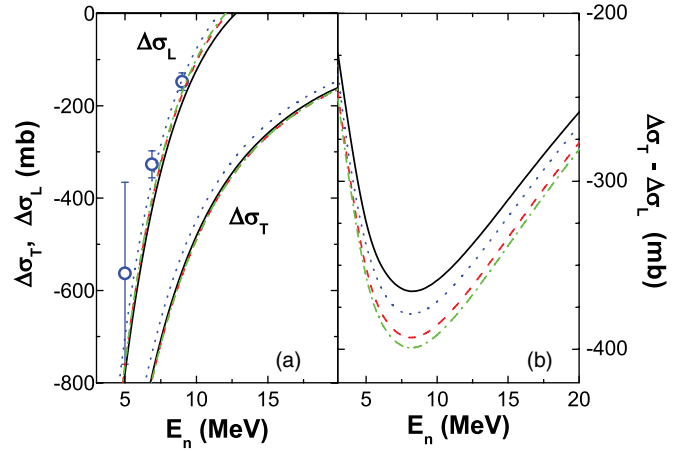

FIG. 6. (Color online) (a) Spin-dependent cross section differences, $\Delta\sigma_L$ and $\Delta\sigma_T$, and (b) their difference $\Delta\sigma_T - \Delta\sigma_L$. Dotted (blue) curves denote the AV18 calculations; dotted-dashed (green) curves, AV18+BR$_{680}$; dashed (red) curves, AV18+BR$_{680}$+SO; solid (black) curves, AV18+BR$_{800}$+C+T+SO. Experimental data of $\Delta\sigma_L$ are from Ref. [26].

In summary, we have studied the effects of spin dependence in nuclear interactions on N-d polarization observables using a 3NF model to be added to the Argonne V$_{18}$ 2NF and the Brazil 2πE-3NF. The 3NF model consists of spin-independent, spin-orbit, and tensor components, which are essential in reproducing the 3N binding energy, the proton vector analyzing power $A_y(\theta)$, and the deuteron tensor analyzing power $T_{21}(\theta)$ in p-d scattering at 3 MeV, respectively. Effects of the 3NF model on some N-d polarization observables at higher energies are examined. The spin-orbit component in the 3NF model plays a significant role in reproducing $A_y(\theta)$. The tensor component has nonnegligible effects in $T_{21}(\theta \approx 90°)$, $A_y(\theta \approx 90°)$, and $K_y^{y'}(\theta \approx 120°)$, although we need more experimental data to confirm whether its effect is favorable. $K_x^{x'}(\theta \approx 120°)$ and $K_z^{z'}(\theta \approx 120°)$ depend on both the spin-orbit and the tensor components. Effects of the tensor component are clearly seen in the spin-dependent n-d cross section differences. Thus, further experimental studies of these observables are expected to improve our knowledge of the spin dependence of three-nucleon forces.

If the 3NF model presented in this work really is successful in explaining all the experimental data, it would be interesting to see what kind of realistic 3NFs are simulated by it. In Ref. [28], an examination of 3NFs arising from the exchange of a pion and a scalar object, such as σ and ω, or a scalar part of two-pion exchange demonstrates that these 3NF types indicate tensor inversion effects that are qualitatively but not quantitatively similar to those of our 3NF model. Of course, this is not conclusive because of the large amount of uncertainty in the description of such processes, and further study is required.

[1] S. A Coon, M. D. Scadron, P. C. McNamee, B. R. Barrett, D. W. E. Blatt, and B. H. J. McKellar, Nucl. Phys. **A317**, 242 (1979).

[2] H. T. Coelho, T. K. Das, and M. R. Robilotta, Phys. Rev. C **28**, 1812 (1983).

[3] A. Kievsky, M. Viviani, and S. Rosati, Phys. Rev. C **64**, 024002 (2001).

[4] A. Kievsky, Phys. Rev. C **60**, 034001 (1999).

[5] S. Ishikawa, M. Tanifuji, and Y. Iseri, Phys. Rev. C **67**, 061001(R) (2003).

[6] S. Ishikawa, M. Tanifuji, and Y. Iseri, in *Proceedings of the 17th International IUPAP Conference on Few-Body Problems in Physics, Durham, North Carolina, 2003*, edited by W. Glöckle and W. Tornow (Elsevier, Amsterdam, 2004), p. S61.

[7] S. Ishikawa, Nucl. Phys. **A463**, 145c (1987).

[8] T. Sasakawa and S. Ishikawa, Few-Body Syst. **1**, 3 (1986).

[9] S. Ishikawa, Few-Body Syst. **32**, 229 (2003).

[10] S. Ishikawa, Few-Body Syst. **40**, 145 (2007).

[11] R. B. Wiringa, V. G. J. Stoks, and R. Schiavilla, Phys. Rev. C **51**, 38 (1995).

[12] S. A. Coon and W. Glöckle, Phys. Rev. C **23**, 1790 (1981).

[13] H. F. Jones and M. D. Scadron, Phys. Rev. D **11**, 174 (1975).

[14] K. Sagara, H. Oguri, S. Shimizu, K. Maeda, H. Nakamura, T. Nakashima, and S. Morinobu, Phys. Rev. C **50**, 576 (1994).

[15] S. Shimizu, K. Sagara, H. Nakamura, K. Maeda, T. Miwa, N. Nishimori, S. Ueno, T. Nakashima, and S. Morinobu, Phys. Rev. C **52**, 1193 (1995).

[16] K. Hatanaka, N. Matsuoka, H. Sakai, T. Saito, K. Hosono, Y. Koike, M. Kondo, K. Imai, H. Shimizu, T. Ichihara, K. Nisimura, and A. Okihana, Nucl. Phys. **A426**, 77 (1984).

[17] W. Tornow, C. R. Howell, M. Alohali, Z. P. Chen, P. D. Felsher, J. M. Hanly, R. L. Walter, G. Weisel, G. Mertens, I. Slaus, H. Witała, and W. Glöckle, Phys. Lett. **B257**, 273 (1991).

[18] W. Tornow, C. R. Howell, R. C. Byrd, R. S. Pedroni, and R. L. Walter, Phys. Rev. Lett. **49**, 312 (1982).

[19] W. Tornow, R. C. Byrd, C. R. Howell, R. S. Pedroni, and R. L. Walter, Phys. Rev. C **27**, 2439 (1983).

[20] K. Fujita, Ph.D thesis (1999), Kyushu University; K. Sagara (private communication).

[21] H. Dobiasch, R. Fischer, B. Haesner, H. O. Klages, P. Schwarz, B. Zeitnitz, R. Maschuw, K. Sinram, and K. Wick, Phys. Lett. **B76**, 195 (1978).

[22] P. Hempen, P. Clotten, K. Hofenbitzer, T. Köble, W. Metschulat, M. Schwindt, W. von Witsch, L. Wätzold, J. Weltz, W. Glöckle, D. Hüber, and H. Witała, Phys. Rev. C **57**, 484 (1999).

[23] L. Sydow, S. Lemaitre, P. Niessen, K. R. Nyga, G. Rauprich, R. Reckenfelderbäumer, S. Vohl, H. Paetz gen. Schieck, H. Witała, and W. Glöckle, Nucl. Phys. **A567**, 55 (1994).

[24] H. Witała, J. Golak, R. Skibiński, W. Glöckle, A. Nogga, E. Epelbaum, H. Kamada, A. Kievsky, and M. Viviani, Phys. Rev. C **73**, 044004 (2006).

[25] S. Ishikawa, M. Tanifuji, and Y. Iseri, Phys. Rev. C **66**, 044005 (2002).

[26] R. D. Foster, C. R. Gould, D. G. Haase, J. M. Kelley, D. M. Markoff, and W. Tornow, Phys. Rev. C **73**, 034002 (2006).

[27] S. Ishikawa, M. Tanifuji, and Y. Iseri, Phys. Rev. C **64**, 024001 (2003).

[28] S. Ishikawa, in *Proceedings of the 18th International IUPAP Conference on Few-Body Problems in Physics, Santos, Brazil, August 21–26, 2006,* edited by L. Tomio, S. Adhikari, and G. Krein, to appear in Nucl. Phys. A.